A Multi-channel Femtoampere-sensitivity Conductometric Array for Biosensing Applications

Amit Gore *, Shantanu Chakrabartty * , Sudeshna Pal †, Evangelyn Alocilja †
goreamit@egr.msu.edu, shantanu@msu.edu, palsudes@msu.edu, alocilja@egr.msu.edu
*Department of Electrical and Computer Engineering
†Department of Biosystems Engineering Michigan State University
East Lansing, MI 48824 USA

***Abstract*— Rapid detection of pathogens using field deployable biosensors requires integrated sensing and data processing. Detection of low concentration of biological agents is possible using accurate and real-time signal characterization devices. This paper presents a multi-channel conductometric array that can detect and measure current up to femtoampere range. The architecture uses a novel semi-synchronous $\Sigma\Delta$ modulation that allows measurement of ultra-small currents by using a hysteretic comparison technique. The architecture achieves higher energy efficiency over a conventional $\Sigma\Delta$ by reducing the total switching cycles of the comparator. A 3 mm $\times$ 3 mm chip implementing a 42 channel potentiostat array has been prototyped in a $0.5\mu m$ CMOS technology. Measured results show 10 bits of resolution, with a sensitivity of upto 50 fA of current. The power consumption of the potentiostat is $11\mu W$ per channel at a sampling rate of 250 kHz. The multi-channel potentiostat has been integrated with a conductometric biosensor for field deployable applications. Results with a *Bacillus Cereus* based biosensor demonstrate the effectiveness of the potentiostat in characterizing different concentration levels of pathogens in real-time.**

I. Introduction

Naturally occurring foodborne disease outbreaks have caused an estimated 76 million illnesses, which include 325,000 hospitalization and 5000 deaths in the United States every year [1]. An estimate by the United States Department of Agriculture (USDA) indicates a loss of $2.9-$6.7 billion due to medical costs and lost productivity due to outbreaks [1]. Rapid detection of pathogens using field deployable biosensors is therefore necessary to ensure effective implementation of preventive measures [2]. Immunosensors are a type of biosensor that are of great interest because of their applicability, specificity and high sensitivity.

An antibody-based conductometric immunosensor that was proposed in [4] used porous filter membranes and have shown a detection limit of 80 CFU/ml (Colony Forming Unit/ml) for bacteria in about 6 minutes. The apparatus has also been successfully demonstrated in detecting as little as 103 cell culture infective dose per milliliter of BVDV (Bovine viral diarrhea virus) antigens (CCID/ml) within 10 minutes [4]. The biosensor shown in fig. (1) is relatively inexpensive to fabricate and easy to operate which makes it an attractive candidate for designing field deployable multi-channel detection systems. For field based applications a true/false type of biosensor is more important which detects presence or absence of pathogens, independent of their relative concentration levels. This is useful especially for zero-tolerance pathogens like E.coli O157:H7 and Salmonella, L. Monacytogens where even small concentration could be proven dangerous because of its virulence and pathogenicity. For instance, the federal EPA standard for E.coli 0157:H7 in water is 40 cells per liter [5]. At such a low concentration of pathogens, a measurement instrument has to be sensitive enough to detect small changes in biosensor response. In [6], the detection accuracy of the biosensor was improved to 10^0 CFU/ml by using time-series classification techniques in conjunction with cross-reactive multi-channel data. It was also shown in [6] that the detection accuracy of the system could be improved further if small changes in impedance can be measured in real-time. This motivates the design of an accurate and highly sensitive multi-channel conductometric array for biosensing applications.

In literature, several multi-channel conductometric and current mode data converters have been proposed for electrochemical measurements. For instance in [7], a $\Sigma\Delta$ approach was used to measure neuro-chemical reactions. An integrating

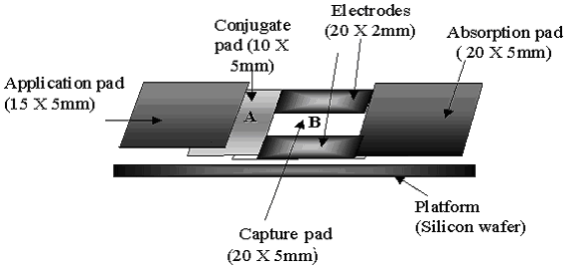

Fig. 1. *Architecture of the immunosensor used in multi-channel biosensor*

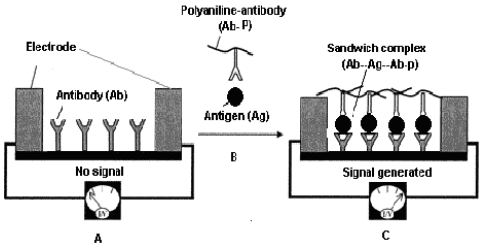

Fig. 2. *Principle of operation of the immunosensor.*

analog-to-digital conversion technique has been used for cyclic voltammetry applications and has demonstrated sensitivity up to picoamperes of current. For a sub-picoampere range of current measurement, noise due to charge injection and substrate coupling becomes a dominant factor. Fundamentally the resolution of data conversion at small currents is limited by thermal noise [8]. In this paper we present an alternative method called *semi-synchronous* $\Sigma\Delta$ modulation that can achieve femtoampere range sensitivity without significantly increasing the conversion time. The architecture uses a novel hysteretic modulation technique in a $\Sigma\Delta$ configuration to reduce the total switching cycles. This configuration alleviates the effect of switching and thermal noise.

This paper is organized as follows: section II describes the architecture and principle of operation of the biosensor. Section III describes the hysteretic $\Sigma\Delta$ algorithm and compares it with traditional $\Sigma\Delta$ formulation. Section IV describes the architecture of a multi-channel conductometric array. Section V summarizes some measured characteristics obtained from the fabricated prototype. Section VI shows measured biosensor data for *Bacillus Cereus*. Section VII concludes with some final remarks.

II. Biosensor: Architecture and principle of operation

The architecture of a single immunosensor as proposed in [3] is shown in fig. (1). It comprises of four different pads: sample application, conjugate, capture, and absorption. Details about fabrication of the biosensor can be found in [3] and its principle of operation is described here briefly. The biosensor uses a capillary action based lateral flow technique to move the liquid sample from one pad to another. Fig. (2) illustrates the principle of operation of the immunosensor. Before the sample is applied, the gap between the electrodes in the capture pad is open [Fig. (2)(a)]. Immediately after sample is applied to the application pad, the solution carrying the antigen flows to the conjugate pad and dissolves the polyaniline-labeled antibody (Ab-P). Polyaniline is a conductive polymer which acts as an electrochemical transducer to convert the bindings into electrical signals [3]. The antibody-antigen binding occurs at the conjugate pad and forms a complex [Fig. (2)(b)]. This complex is carried into the capture pad containing the immobilized antibody. A second antibody-antigen reaction occurs and forms a sandwich [Fig. (2)(c)]. Polyaniline in the sandwich forms a molecular wire and bridges the two electrodes. The polymer structures extend out to bridge adjacent cells and leads to impedance change between the electrodes [9]. The impedance change is determined by the number of antigen-antibody bindings which is related to the antigen concentration in the sample. The unbound non-target organisms are subsequently separated by capillary flow to the absorption membrane. The impedance change is then sensed as an electrical current by an integrated conductometric array.

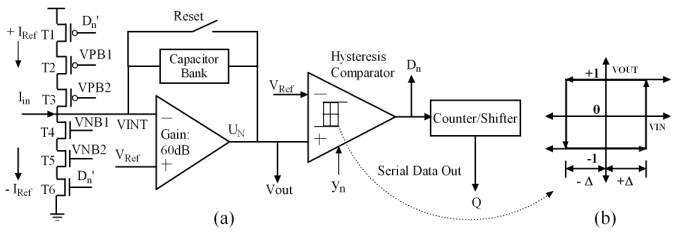

Fig. 3. *Schematic of the proposed semi-synchronous* $\Sigma\Delta$ *converter*

III. Hysteretic $\Sigma\Delta$ Algorithm

The architecture of a hysteric $\Sigma\Delta$ is shown in fig. (3)(a). The topology is very similar to the current mode architecture presented in [7] except for a hysteretic comparator. The input-output characteristic of the comparator is shown in fig. (3)(b), where Δ denotes its hysteresis level. If the output voltage level of the integrator is denoted by U_n, where $n = 1, .., N$ is the number of clock cycles, then the $\Sigma\Delta$ step is given by [11]:

$$U_n = U_{n-1} + (\frac{I_{in}}{I_{Ref}} - D_n)\frac{I_{Ref}T_{CLK}}{C} \quad (1)$$

$$D_n = sign(U_{n-1} + D_{n-1}\Delta). \quad (2)$$

where $sign(.) \in \{+1, -1\}$ denotes a signum function and I_{in} is the input current. I_{Ref} is the reference current, T_{CLK} is the clock period for each $\Sigma\Delta$ step and C is the feedback capacitance of the integrator. Compared to conventional $\Sigma\Delta$ operation, the digital output at time instant n, D_n is correlated with digital outputs at previous clock cycles.

Note that the integrator output U_n in equation 1 is bounded according to the following relation:

$$|U_n| \leq \Delta + \frac{2I_{Ref}T_{CLK}}{C}. \quad (3)$$

Even though magnitude of the $\Sigma\Delta$ residue has large dynamic range, the following result shows that the resolution of hysteretic $\Sigma\Delta$ conversion can be made equal to conventional $\Sigma\Delta$ conversion with inclusion of a compensation step. Introducing auxiliary variables $V_n = U_n + D_n\Delta$ the expression in equation 1 after N cycles can be written as:

$$\frac{V_N}{N} = (\frac{I_{in}}{I_{Ref}} - \frac{1}{N}\sum_{n=1}^{N} D_n)\frac{I_{Ref}T_{CLK}}{C} + \frac{(D_N - D_0)\Delta}{N}. \quad (4)$$

The recursion 4 is composed of a $\Sigma\Delta$ step and a correlation step due to hysteresis. Thus the residue of the hysteretic $\Sigma\Delta$ conversion is a combination of residue due to conventional $\Sigma\Delta$ conversion and a hysteretic residue $H_N = \frac{(D_N - D_0)\Delta}{N}$. The effect of the hysteretic residue can be eliminated by introducing an extended counting step which counts additional clock cycles if $D_N \neq D_0$.

From equation 4, it can be seen that the error due to hysteretic residue is eliminated. Since the extended counting step is an asynchronous procedure, overhead is incurred for storing the additional number of clock cycles used in extended conversion. An alternative method that avoids this overhead

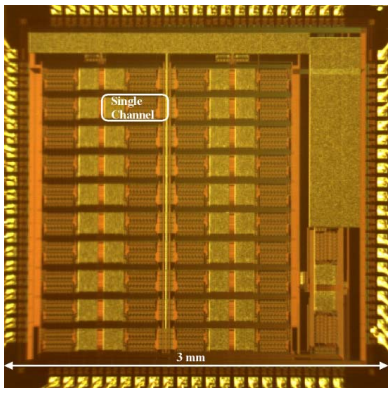

Fig. 4. *Microphotograph of the 42 channel conductometric array*

is to quantize the output of an integrator U_N directly after N cycles using any A/D conversion method. Following N hysteretic $\Sigma\Delta$ clock cycles, an integrating A/D conversion is performed on the residue U_N by switching off the input current I_{in}. The recursion 1 is then given by

$$U_n = U_{n-1} - D_n^* \frac{I_{Ref} T_{CLK}}{C} \tag{5}$$

where D_n^* denotes the extended bits obtained using the integrating A/D conversion. The recursion 5 stops when the condition $D_n^* = D_{n-1}^*$ is satisfied. The final reconstructed (quantized) output is given by $\hat{I_{in}} = \frac{1}{N}(\sum_{n=1}^{N} D_n + \sum_{k=1}^{K} D_k^*)$, where K is total extended cycles of recursion 5.

IV. Hysteretic $\Sigma\Delta$ Architecture

Fig. (3) shows the schematic of the proposed current mode hysteretic $\Sigma\Delta$ converter. It consists of cascoded transistors $T_2 - T_5$ for generating current references $\pm I_{Ref}$. Multiplication of reference current I_{Ref} by digital bit D_n is implemented using switches T_1, T_6 connected to the source of the cascoded transistors. Switching at the source as opposed to switching at the drain reduces channel charge injection and clock feed-through at the integration node V_{INT}. A standard folded cascode opamp has been used to implement the integrator and provides $60dB$ open loop gain. As opposed to cascoded inverter based implementations [7] the opamp allows adjustment of the reference potential V_{INT} that can be varied for different electrochemical experiments. A digitally programmable capacitor bank is used for integration and is also used for adjusting the integration period.

The hysteretic comparator is implemented using a basic differential pair with current starved inverters. The positive hysteresis level $+\Delta$ and the negative hysteresis level $-\Delta$ can be adjusted based on the range of input current. The hysteresis levels are also determined by ambient noise levels. A 16 bit current starved counter/shifter has been implemented using the building blocks described in [10]. In the multi-channel configuration the counters can be daisy-chained and data can be accessed serially.

TABLE I

Specification: Multi-channel conductometric array chip

Parameters	Values
Technology	0.5 μm 2P3M CMOS
Size	3 mm $\times$ 3 mm
Supply	3.3 V
Channels	42
Input Current Range	-100nA to 100nA
Resolution	10 bits
Sensitivity	50fA
Power dissipation per channel	11 μW at 250 kHz
Energy per quantization level	0.045 pJ
Active Area per channel	0.085 mm^2

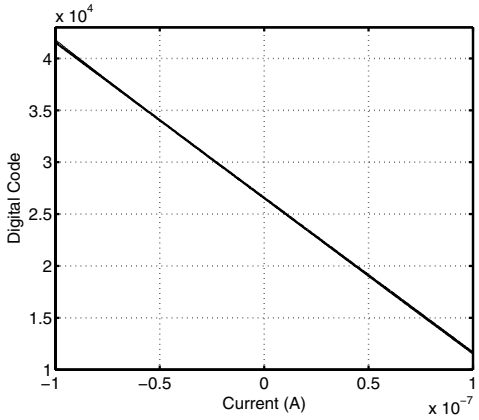

Fig. 5. *ADC output for current range from -100nA to +100nA in 1000 steps*

V. Measured Chip Results

A 42 channel conductometric array chip has been fabricated in a $0.5\mu m$ CMOS process. The size of the prototype is 3 mm $\times$ 3 mm and its microphotograph is shown in fig. (4). Table I summarizes the specification of the chip. Fig. (5) shows digital output of the conductometric ADC channel when the input current was swept from $-100nA$ to $100nA$ in steps of $100pA$. Fig. (6) compares the power dissipated by the semi-synchronous converter with a conventional $\Sigma\Delta$ converter at different sampling frequencies. The plot shows that the power consumed by the semi-synchronous converter is almost half of the power consumed by the conventional $\Sigma\Delta$ converter. The power efficiency improves as the sampling frequency increases. This can be attributed to reduced switching cycles and is determined by the hysteresis level of a comparator. For a sampling rate of 250 kHz, the power dissipation of a single channel is $11\mu W$. To demonstrate femtoampere range sensitivity, an on-chip pMOS transistor was used for current generation. The set-up avoided unneccesary coupling from external noise sources, which is critical for ultra-small current measurements. Fig. (7) shows the log linear plot of digitized output as the gate of the pMOS transistor is varied. Gate voltages were mapped to current values using an external pico-ammeter. Fig. (7) shows that the prototype can measure sub-threshold currents of the pMOS transistor up to femtoampere

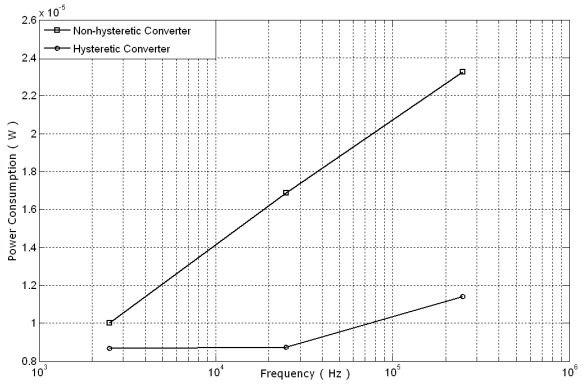

Fig. 6. *Comparison of power dissipated by a semi-synchronous $\Sigma\Delta$ with a conventional $\Sigma\Delta$ for different sampling frequency*

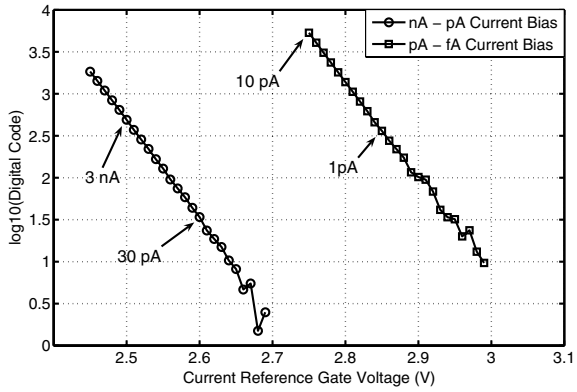

Fig. 7. *Measurement of sub-threshold characteristics of a pMOS transistor using the proposed current mode ADC.*

range.

VI. Biosensor Measurements

The setup for measuring concentration levels of *Bacillus Cereus* using an array of biosensors is shown in Fig. (8). Each biosensor was exposed to different concentration (dilution) levels. The concentration levels of pathogens chosen for this experiment were control(blank) solution, 10^3, 10^4, 10^5 and 10^6 CFU/ml. Fig. (9) shows the measured impedance plots for different concentration levels of the pathogens. Significant impedance variations were observed between 2 to 3 minutes from the start of reaction, and can be used for detecting different concentration levels. All dilutions show distinctive impedance change during the 120 second to 180 second period.

VII. Conclusion

In this paper we introduced a novel current mode hysteretic $\Sigma\Delta$ converter and have demonstrated its sensitivity up to femtoampere range of currents. A multi-channel potentiostat has been fabricated with the proposed architecture and its functionality has been verified for a real-life biosensing application. The new architecture offers a low power current measurement technique. Currently we are working on integrating the

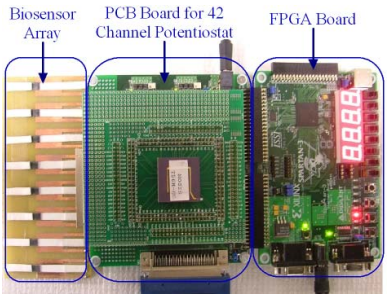

Fig. 8. *Experimental setup for biosensor measurement*

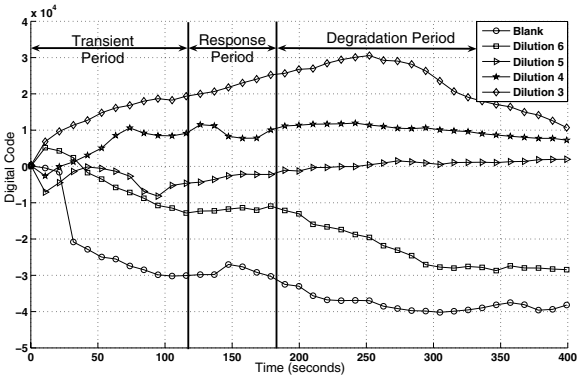

Fig. 9. *Biosensor data for different concentrations of Bacillus Cereus*

multi-channel architecture with radio-frequency identification (RFID) tags, that will be integrated with the biosensor array and facilitate remote interrogation and operation.

References

[1] S. M. Radke, E. C. Alocija, " A microfabricated biosensor for detecting foodborne bioterrorism agents, " IEEE sensors J., vol. 5 no. 4, pp. 744-750, Aug. 2005.

[2] Food and Drug Administration, " Bacteriological Analytical Manual. 8th ed., " Arlington, VA: Association of Analytical Chemists, 2000.

[3] Z. Muhammad-Tahir and E. C. Alocilja, "Fabrication of a disposable biosensor for Escherichia coli o157:H7 detection, " IEEE sensors Journal , vol. 3 (4), pp. 345-351, 2003

[4] Z. Muhammad-Tahir and E. C. Alocilja, "Rapid Detection of Bovine viral diarrhea virus as surrogate of bioterrorism agents, " IEEE Sensors Journal, vol. 4, pp. 757-762, 2005.

[5] J. M. Jay, Moden Food Microbiology. Aspen publishers, Inc. Gaithersburg, MD. 2000

[6] Yueming. Z, Chakrabartty. S, Muhammad-Tahir. Z,Pal. S, and Alocilja. E.C, " Spatio-temporal Processing for Multi-channel Biosensors using Support Vector Machines," *Under Preparation*.

[7] Stanacevic, M.; Murari, K.; Cauwenberghs, G.; Thakor, N.; "16-channel wide-range VLSI potentiostat array", Biomedical Circuits and Systems, 2004 IEEE International Workshop on 1-3 Dec. 2004

[8] Yang, H.Y. and Sarpeshkar, R. "A time-based energy-efficient analog-to-digital converter" Solid-State Circuits, IEEE Journal of Volume 40, Issue 8, Aug. 2005 Page(s):1590 - 1601

[9] T. A. Sergeyeva, Lavrik, N.V., Rachkov, A.E. . "Polyaniline label-based Conductimetric Sensor for IgG detection," Sensors and Actuators B, vol. 34, pp. 283-288, 1996.

[10] Schienle, M.; Paulus, C.; Frey, A.; Hofmann, F.; Holzapfl, B.; Schindler-Bauer, P.; Thewes, R.;"A fully electronic DNA sensor with 128 positions and in-pixel A/D conversion", Solid-State Circuits, IEEE Journal of Volume 39, Issue 12, Dec. 2004

[11] J. Candy and G. Temes, Oversampling delta-sigma data converters, IEEE Press, 1991.